Effect of Terminal Modifications on the Adsorption and Assembly of hIAPP(20-29)

Roozbeh Hajiraissi,[†] Marcel Hanke,[†] Alejandro Gonzalez Orive,[†] Belma Duderija,[†] Ulrike Hofmann,[‡] Yixin Zhang,[‡] Guido Grundmeier,[†] and Adrian Keller[†]*

† Technical and Macromolecular Chemistry, Paderborn University, Warburger Str. 100, 33098 Paderborn, Germany.

‡ B CUBE - Center for Molecular Bioengineering, Technische Universität Dresden, Arnoldstr. 18, 01307 Dresden, Germany.

ThT fluorescence spectra

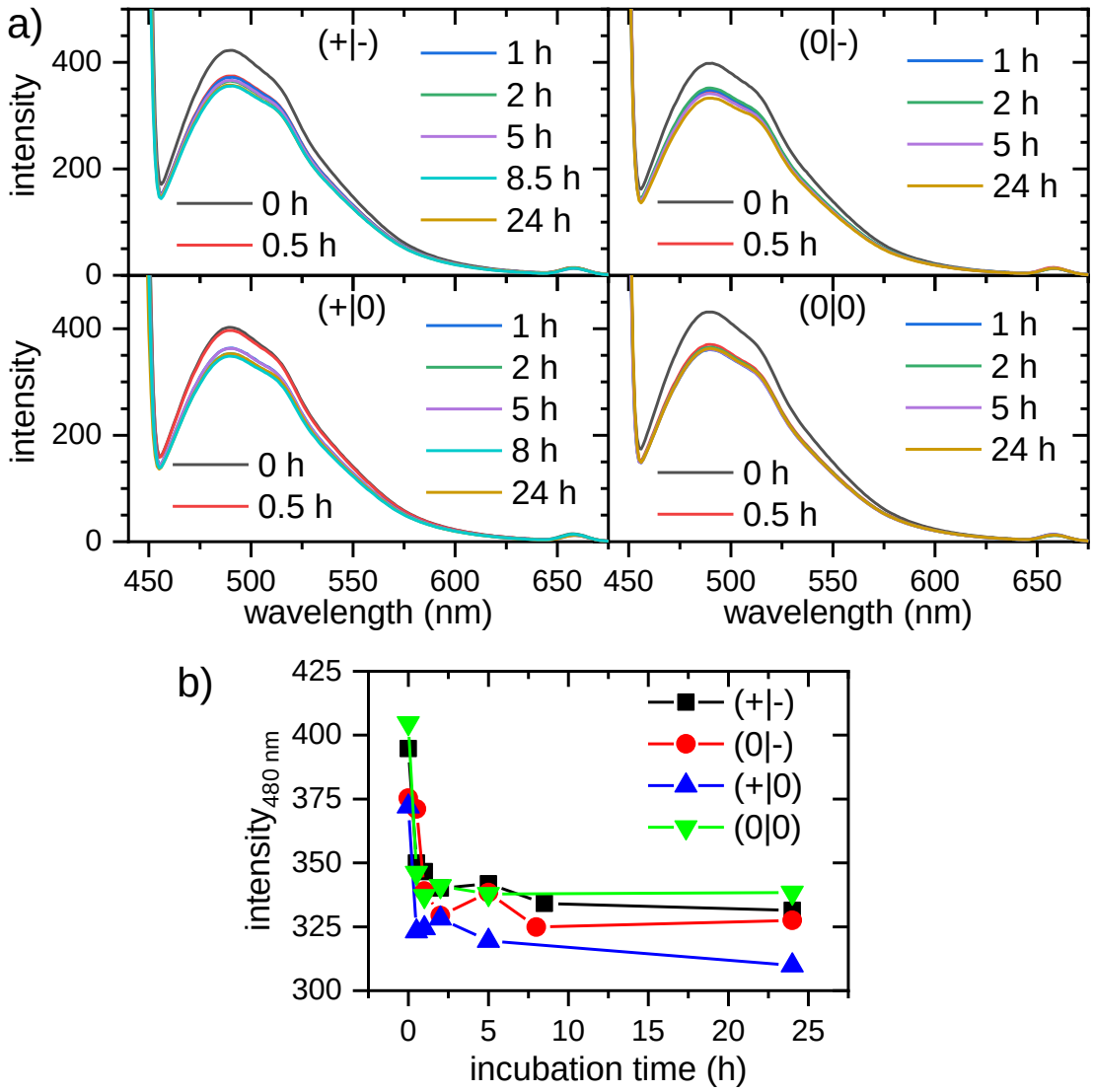

Figure S1. *a) ThT fluorescence spectra for the different hIAPP(20-29) fragments in bulk solution (PBS, pH 7.5, 37°C, λ_{ex} = 440 nm) recorded after different times of incubation. b) Corresponding fluorescence intensities (λ_{em} = 480 nm) as a function of incubation time.*

Additional AFM images for assembly in bulk solution

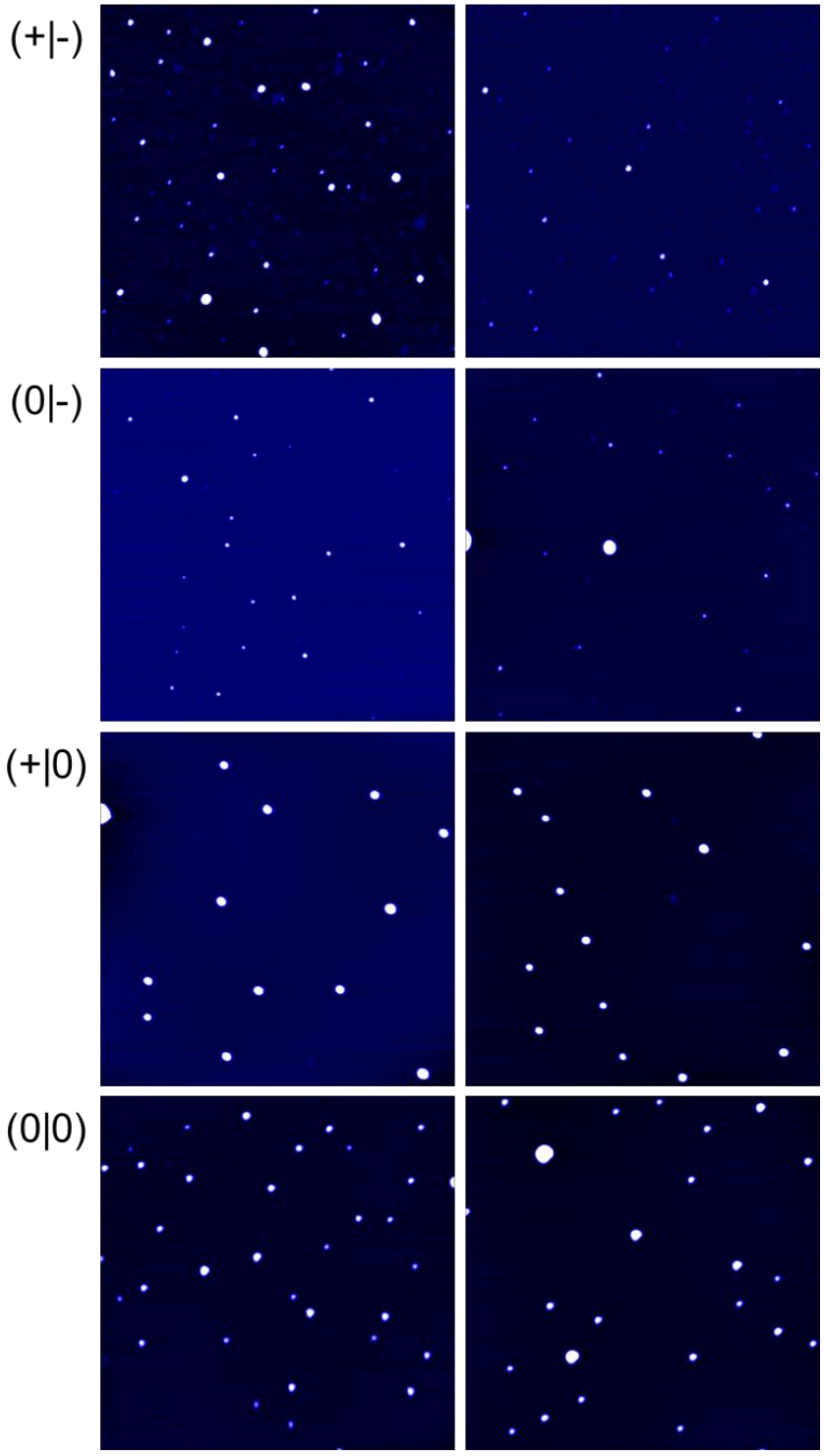

Figure S2. *Additional AFM images (2 x 2 µm²) of the assembled hIAPP(20-29) aggregates recorded after 24 h incubation without ThT. The z-scales are 5 nm for all images.*

Different overtones recorded in the QCM-D measurements

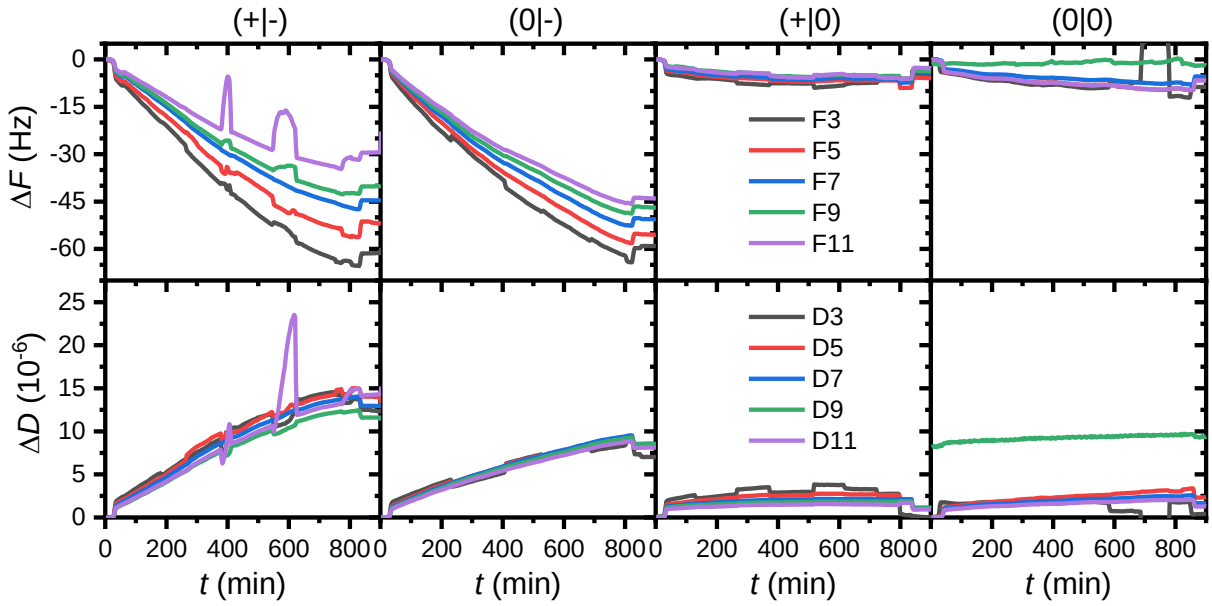

Figure S3. *ΔF and ΔD results (overtones 3 to 11) for the adsorption of the different hIAPP(20-29) fragments at the NH_2-terminated SAM.*

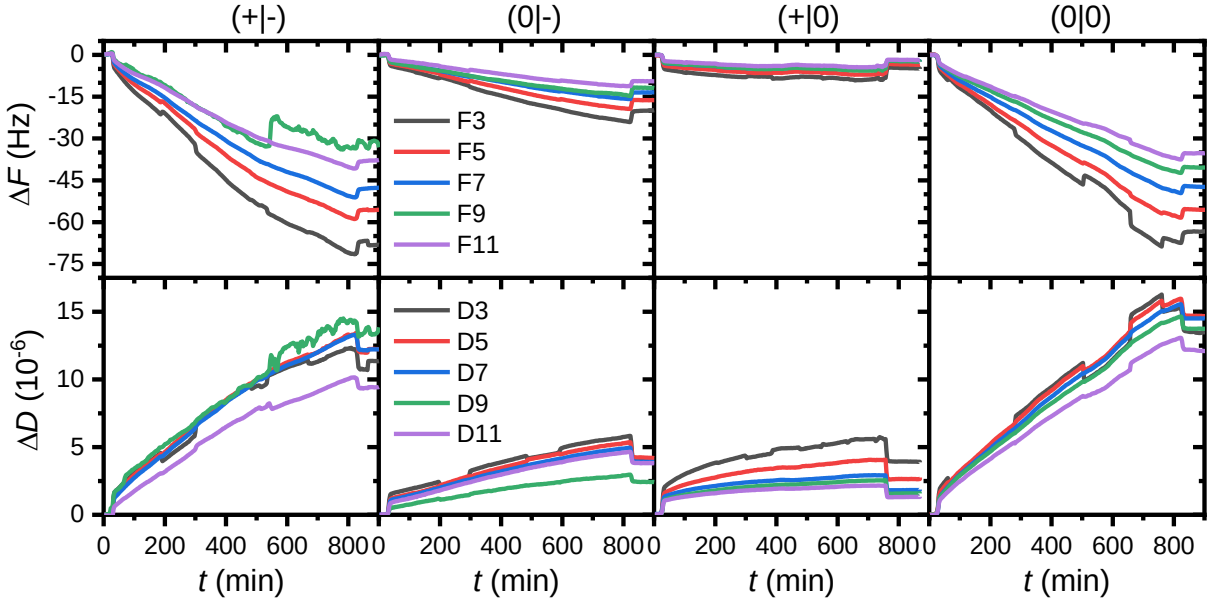

Figure S4. *ΔF and ΔD results (overtones 3 to 11) for the adsorption of the different hIAPP(20-29) fragments at the COOH-terminated SAM.*

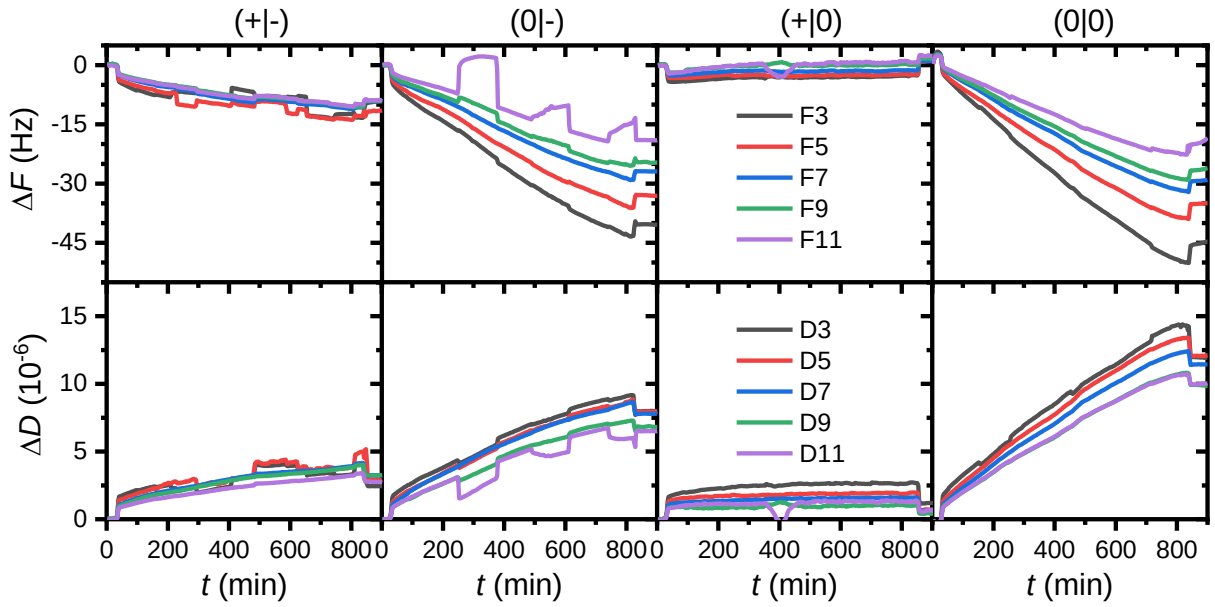

Figure S5. *ΔF and ΔD results (overtones 3 to 11) for the adsorption of the different hIAPP(20-29) fragments at the OH-terminated SAM.*

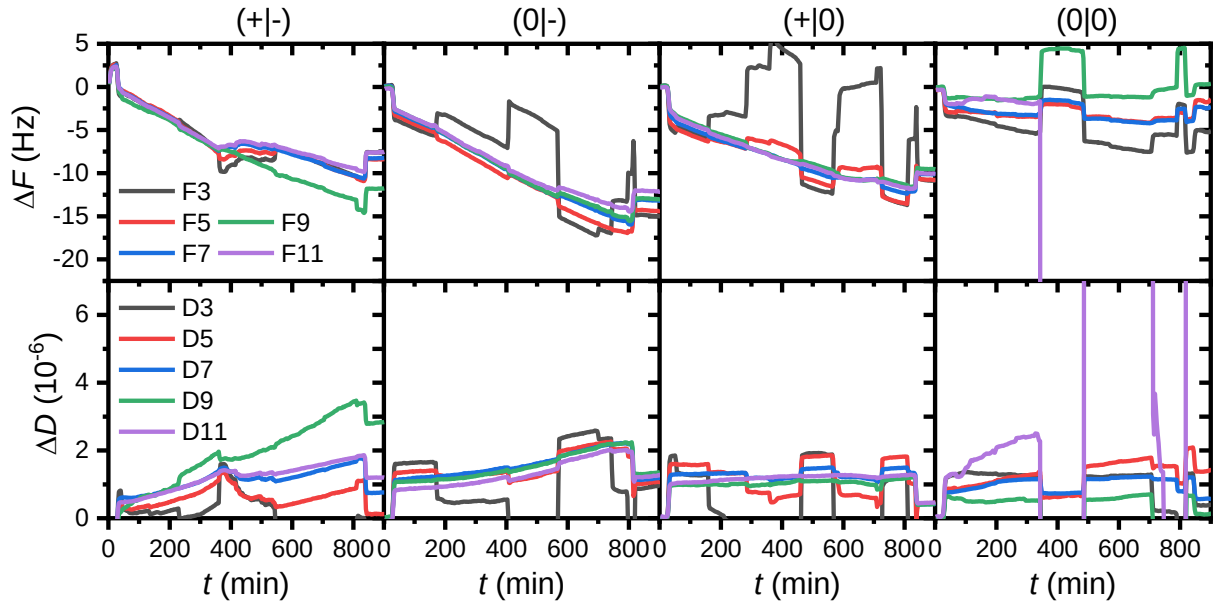

Figure S6. *ΔF and ΔD results (overtones 3 to 11) for the adsorption of the different hIAPP(20-29) fragments at the CH_3-terminated SAM.*

AFM images of the different adsorbate films at NH_2, COOH, and OH SAMs

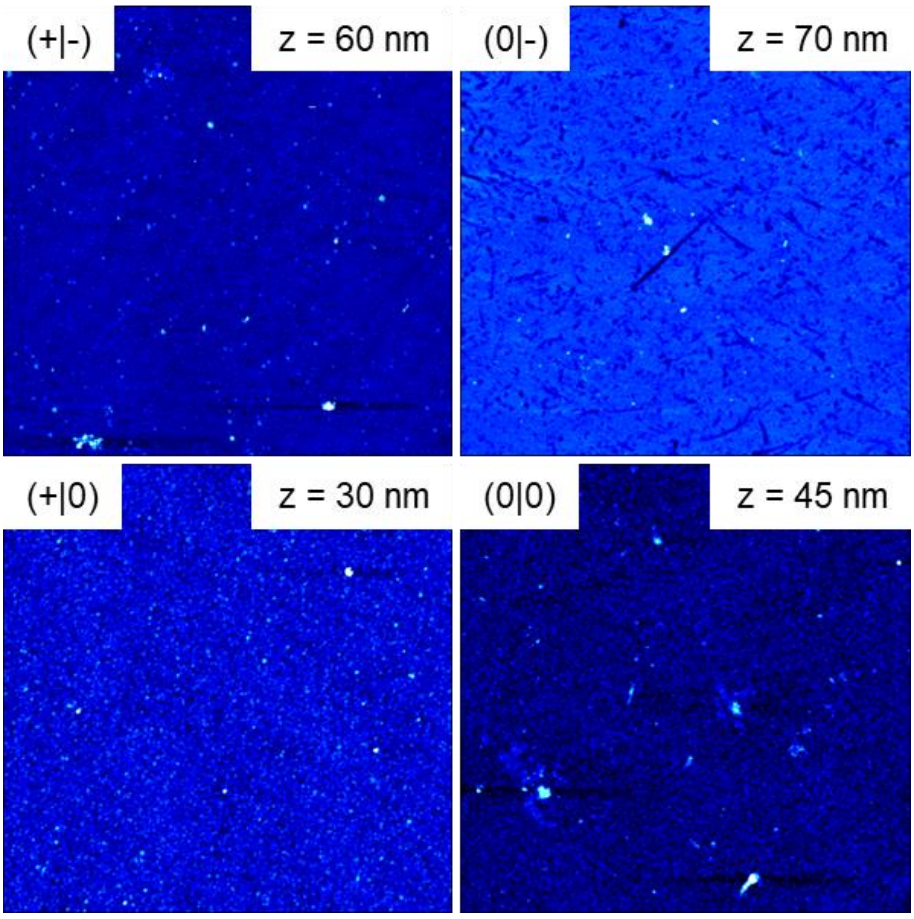

Figure S7. *AFM images (10 × 10 μm^2) of the adsorbed fragments on the NH_2 SAM recorded after the end of the QCM-D measurements. The ranges of the z-scales are given in the images.*

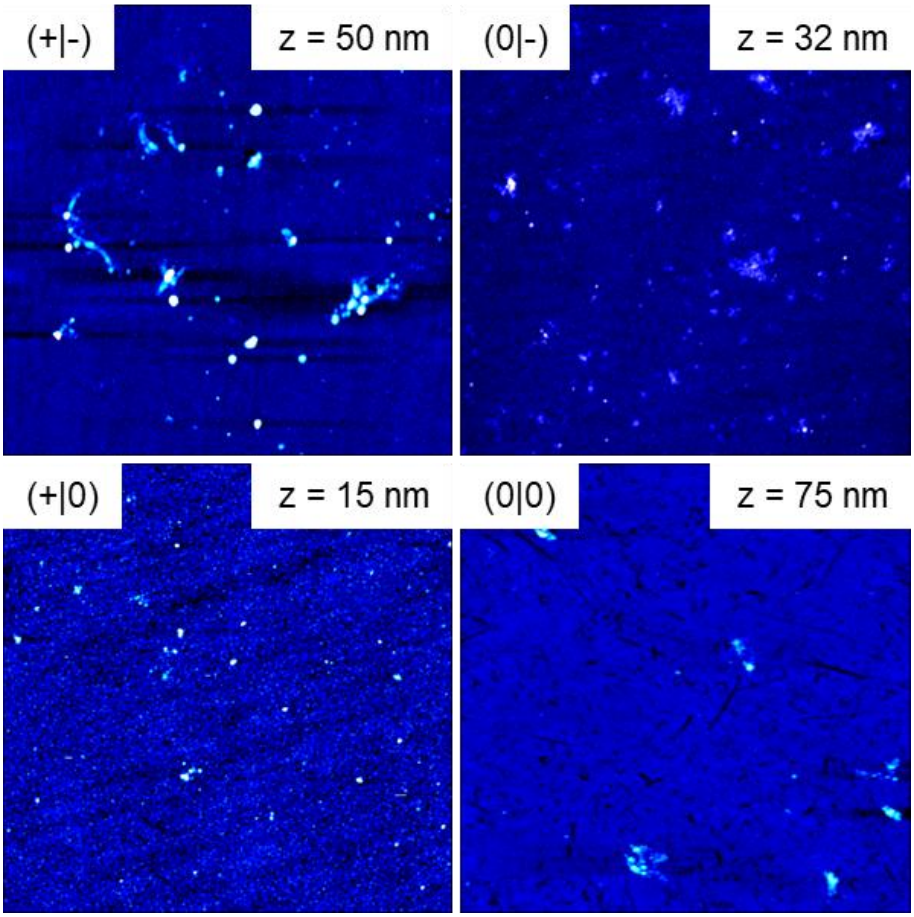

Figure S8. *AFM images (10 × 10 μm^2) of the adsorbed fragments on the COOH SAM recorded after the end of the QCM-D measurements. The ranges of the z-scales are given in the images.*

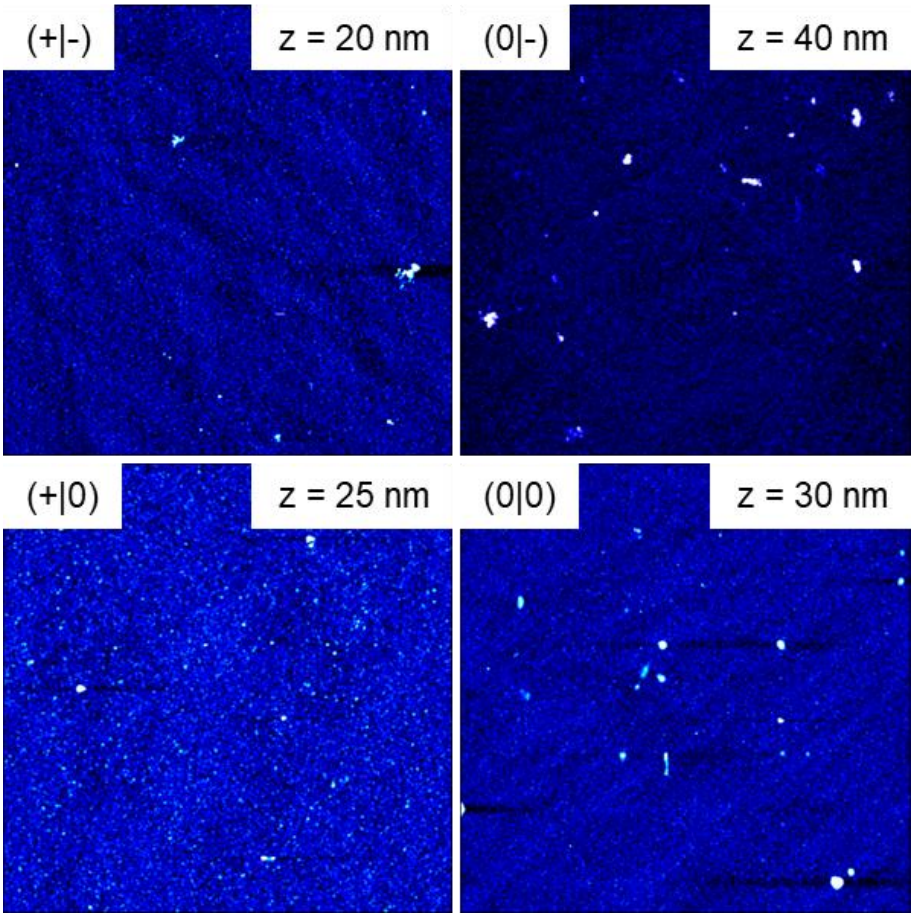

Figure S9. *AFM images (10 × 10 μm^2) of the adsorbed fragments on the OH SAM recorded after the end of the QCM-D measurements. The ranges of the z-scales are given in the images.*

Deconvolution of PM-IRRA spectra

The PM-IRRAS technique has been traditionally used for the accurate assessment of the secondary structure exhibited by both polypeptides and proteins from their characteristic amide contributions.[1,2] The amide I peak originates mainly from backbone C=O stretching vibrations and shows frequencies in the range of 1700 – 1600 cm^{-1}. The exact band position is determined by the backbone conformation and, consequently, resembles the secondary structure of the protein. The amide II band reflects a combination of backbone N-H bending and C-N stretching and has frequencies between 1580 and 1510 cm^{-1}. We might also associate the position of the latter with the secondary structure of the protein, but the analysis would necessarily be more complex.[3] These amide signatures, *i.e.*, the amide I band centered at 1655 cm^{-1} and amide II at 1550 cm^{-1},[4] appear slightly overlapped in some PM-IRRA spectra. A certain degree of overlapping between amide I and amide II bands has previously been reported for the amyloidogenic Josephin domains of ataxin-3 assembled into oligomers and fibrils.[5] In general, the amide I band (after subtraction of the amide II contribution) is essentially centered at 1620 – 1630 cm^{-1}, characteristic of parallel β-sheet conformations, accompanied by a small peak at 1670 cm^{-1} corresponding to β-turns. In some occasions, a smaller component at 1690 cm^{-1} can be detected as well, which we attribute to antiparallel β-sheets.[6]

The amide I signature exhibited by the different hIAPP(20-29) fragments shows common features which are discussed in detail in the following. Three main moieties in the range of 1610 – 1635 cm^{-1} have been observed, absorbing at approximately 1610 – 1615, 1620 – 1625, and 1634 cm^{-1}, all of them corresponding to vibrational motions of the backbone amide moieties in parallel β-sheet conformations, thus suggesting that monomers in the aggregates could be arranged into different secondary structural architectures and/or aggregation states. The latter would comprise of

oligomers (from dimers to multimers), protofibrils, and mature fibrils of different morphology. In this regard, it has been shown that the intermediate frequency β-sheet component, *i.e.*, at 1620 – 1625 cm^{-1}, can be attributed to an extended multi-stranded intermolecular hydrogen-bonded β-sheet configuration (cross-β architecture found in amyloid-like fibrils).[3,7,8] Additionally, the β-sheet component at higher frequencies, 1634 cm^{-1}, would correspond to shorter and more disordered fibril units, if present.[9] More recently, it has been shown for $A\beta_{1-40}$ and $A\beta_{1-42}$ polypeptides that contributions in the β-sheet range close to 1610 cm^{-1} can be attributed to the occurrence of very stable amyloid fibrils. This finding would open the door to an efficient FTIR-based distinction between amyloid fibrils and β-sheet-rich aggregated oligomers and protofibrils, which more likely appear at 1625 cm^{-1}.[10] Nevertheless, this contribution at 1610 cm^{-1} is not easy to be deconvoluted from the broader and more intense 1625 cm^{-1} peak. The enrichment in the parallel β-sheet content has been traditionally correlated to the aggregated nature of the sample and in particular the formation of amyloid fibrils, whilst an increase in the antiparallel β-sheet has been mostly attributed to the aggregation of oligomers. In this regard, Cerf *et al*. used ATR to unambiguously demonstrate that although both Aβ fibrils and oligomers exhibit a predominant β-sheet structural conformation, only the oligomers show antiparallel β-sheet conformations.[6] In this regard, it has been stated that these Aβ oligomers were composed of β-strands mostly in an antiparallel organization.[7] This behaviour has also been reported for a significant number of other proteins, polypeptides, and fragments, as reviewed by Sarroukh *et al*.[3] On the other hand, more recently, using nano-IR, Ruggeri *et al*. identified a significant increase in the antiparallel β-sheet contribution for the adsorption of Josephin domains of ataxin-3 (1-182) onto APTES-modified mica substrates (positively charged), when comparing native oligomers to misfolded oligomers, which turned out to be even higher for amyloid fibrils.[5]

The detailed deconvolution of the PM-IRRA spectra and the resulting secondary structure contents of the different hIAPP(20-29) fragments assembled in bulk solution and at the different SAM-modified gold surfaces are given in figures S10 – S14 and tables S1 – S5.

Bulk solution

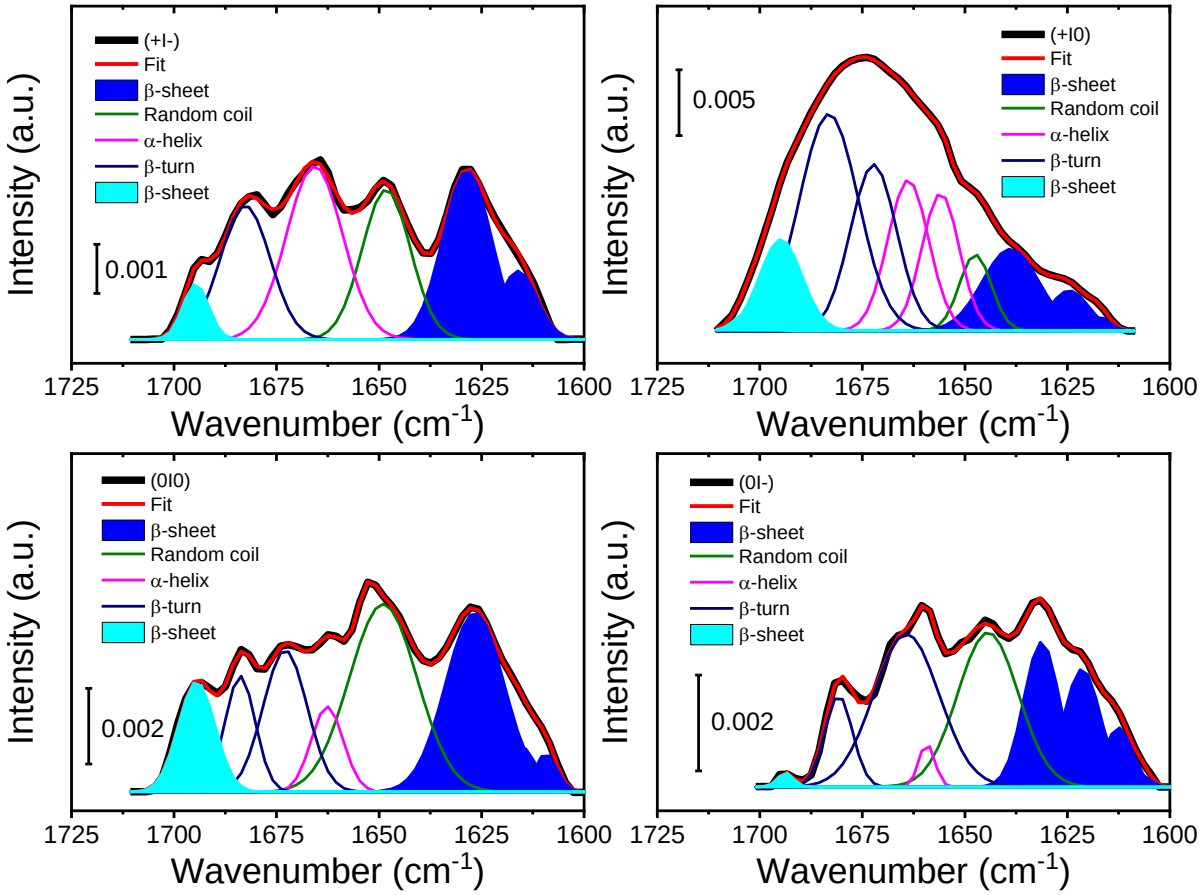

Figure S10. *Deconvolution of the PM-IRRA spectra in the amide I region recorded for the different hIAPP(20-29) fragments assembled in bulk solution: native (upper left panel), amidated (upper right panel), acetylated and amidated (lower left panel) and acetylated (lower right panel), respectively. Black lines correspond to the experimental data while red lines represent the sums of the fitted components.*

Table S1. *Secondary structure contents obtained for the deconvolution of the PM-IRRA spectra registered for the different hIAPP(20-29) fragments assembled in bulk solution.*

	Native (+|-)			
Component	**Position (cm^{-1})**	**Percentage (%)**	**total (%)**	**Amide I area**
β-sheet	1616	7.11	29.94	0.23105
β-sheet	1629	22.83		
Random coil	1648	20.5	20.5	
α-helix	1665	27.03	27.03	
β-turn	1682	18.57	18.57	
β-sheet	1695	3.95	3.95	
	Amidated (+|0)			
Component	**Position (cm^{-1})**	**Percentage (%)**	**total (%)**	**Amide I area**
β-sheet	1617	0.62	14.31	1.06218
β-sheet	1625	3.47		
β-sheet	1637	10.22		
Random coil	1647	5.40	5.40	
α-helix	1656	11.63	25.30	
α-helix	1663	13.67		
β-turn	1672	17.03	45.35	
β-turn	1682	28.31		
β-sheet	1695	9.64	9.64	
	Acetylated and amidated (0|0)			
Component	**Position (cm^{-1})**	**Percentage (%)**	**total (%)**	**Amide I area**
β-sheet	1610	1.98	29.55	0.34539
β-sheet	1615	2.92		
β-sheet	1627	24.64		
Random coil	1649	29.98	29.98	
α-helix	1662	8.08	8.08	
β-turn	1673	14.64	22.93	
β-turn	1684	8.29		
β-sheet	1694	9.46	9.46	
	Acetylated (0|-)			
Component	**Position (cm^{-1})**	**Percentage (%)**	**total (%)**	**Amide I area**
β-sheet	1614	4.82	32.26	0.22231
β-sheet	1621	12.47		
β-sheet	1631	14.96		
Random coil	1644	27.01	27.01	
α-helix	1658	3.46	3.46	
β-turn	1667	28.88	36.18	
β-turn	1680	7.30		
β-sheet	1694	1.09	1.09	

Positively charged NH_2-terminated SAM

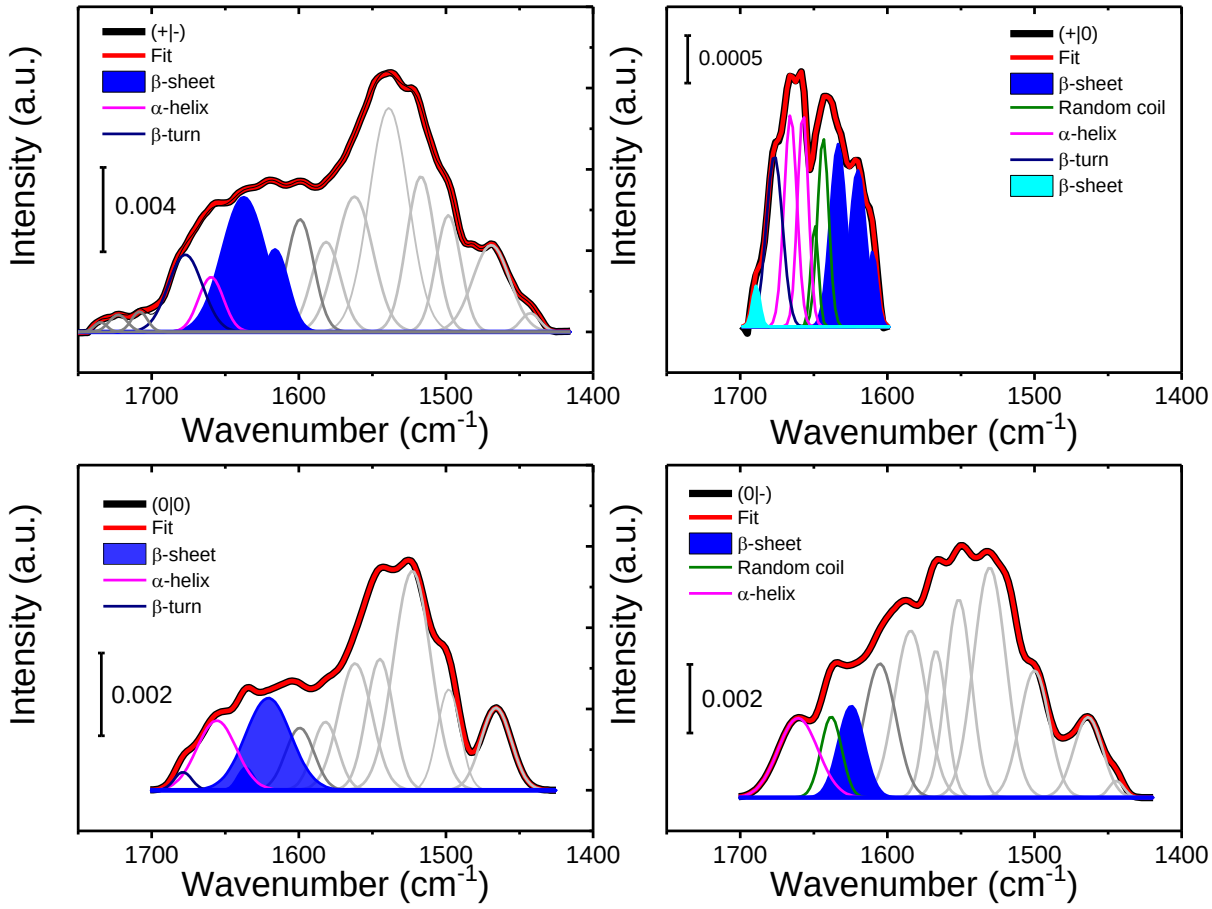

Figure S11. *Deconvolution of the PM-IRRA spectra in the amide I region recorded for the different hIAPP(20-29) fragments assembled at the NH_2-terminated SAM: native (upper left panel), amidated (upper right panel), acetylated and amidated (lower left panel) and acetylated (lower right panel), respectively. Black lines correspond to the experimental data while red lines represent the sums of the fitted components.*

Table S2. *Secondary structure contents obtained for the deconvolution of the PM-IRRA spectra registered for the different hIAPP(20-29) fragments assembled at the NH_2-terminated SAM.*

	Native (+|-)			
Component	**Position (cm^{-1})**	**Percentage (%)**	**total (%)**	**Amide I area**
β-sheet	1616	18.86	66.93	0.51002
β-sheet	1635	48.07		
α-helix	1660	11.27	11.27	
β-turn	1678	21.80	21.80	
	Amidated (+|0)			
Component	**Position (cm^{-1})**	**Percentage (%)**	**total (%)**	**Amide I area**
β-sheet	1611	4.18	35.81	0.16024
β-sheet	1620	14.80		
β-sheet/ R. coil	1633	16.83		
Random coil	1644	12.36	16.85	
Random coil	1650	4.49		
α-helix	1658	13.57	29.24	
α-helix	1665	15.67		
β-turn	1677	16.21	16.21	
β-sheet	1690	1.89	1.89	
	Acetylated and amidated (0|0)			
Component	**Position (cm^{-1})**	**Percentage (%)**	**total (%)**	**Amide I area**
β-sheet	1620	55.02	59.66	0.15864
β-sheet	1635	4.64		
Random coil	-	0	0	
α-helix	1655	36.08	36.08	
β-turn	1678	4.26	4.26	
	Acetylated (0|-)			
Component	**Position (cm^{-1})**	**Percentage (%)**	**total (%)**	**Amide I area**
β-sheet	1624	32.84	32.84	0.18507
Random coil	1640	23.28	23.28	
α-helix/ β-turn	1660	43.88	43.88	
β-turn	-	0	0	

Negatively charged COOH-terminated SAM

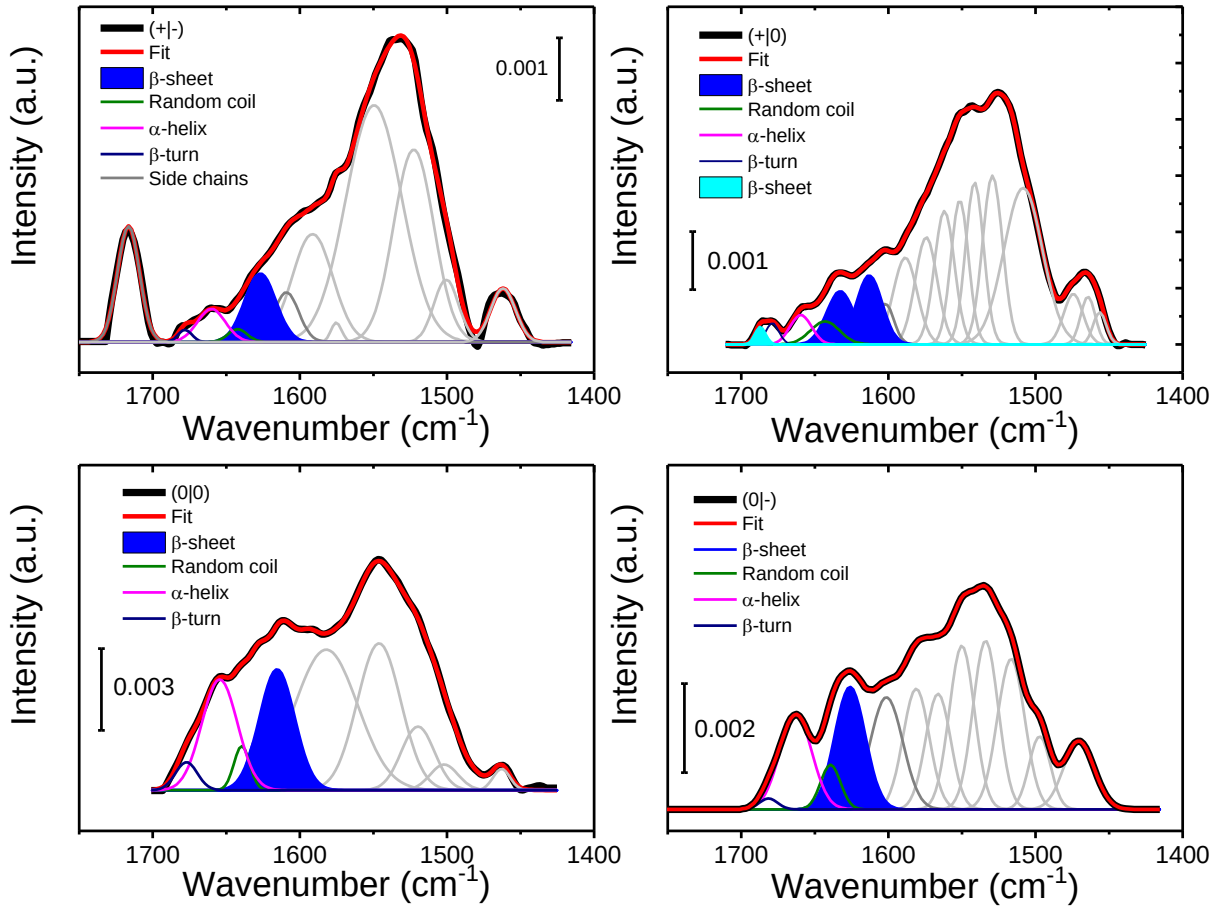

Figure S12. *Deconvolution of the PM-IRRA spectra in the amide I region recorded for the different hIAPP(20-29) fragments assembled at the COOH-terminated SAM: native (upper left panel), amidated (upper right panel), acetylated and amidated (lower left panel) and acetylated (lower right panel), respectively. Black lines correspond to the experimental data while red lines represent the sums of the fitted components.*

Table S3. *Secondary structure contents obtained for the deconvolution of the PM-IRRA spectra registered for the different hIAPP(20-29) fragments assembled at the COOH-terminated SAM.*

	Native (+|-)			
Component	**Position (cm^{-1})**	**Percentage (%)**	**total (%)**	**Amide I area**
β-sheet	1627	61.45	61.45	0.04884
Random coil	1642	7.14	7.14	
α-helix	1660	26.60	26.60	
β-turn	1678	4.80	4.80	
	Amidated (+|0)			
Component	**Position (cm^{-1})**	**Percentage (%)**	**total (%)**	**Amide I area**
β-sheet	1613	35.70	64.52	0.0754
β-sheet	1632	28.82		
Random coil	1644	13.48	13.48	
α-helix	1660	12.64	12.64	
β-turn	1679	5.68	5.68	
β-sheet	1688	3.68	3.68	
	Acetylated and amidated (0|0)			
Component	**Position (cm^{-1})**	**Percentage (%)**	**total (%)**	**Amide I area**
β-sheet	1615	41.17	49.21	0.32557
β-sheet	1629	8.08		
Random coil	1640	6.73	11.4	
α-helix	1655	38.07	64.7	
β-turn	1677	5.94	10.1	
	Acetylated (0|-)			
Component	**Position (cm^{-1})**	**Percentage (%)**	**total (%)**	**Amide I area**
β-sheet	1622	47.56	47.56	0.15602
Random coil	1645	11.28	11.28	
α-helix	1662	38.63	38.63	
β-turn	1682	2.53	2.53	

Polar OH-terminated SAM

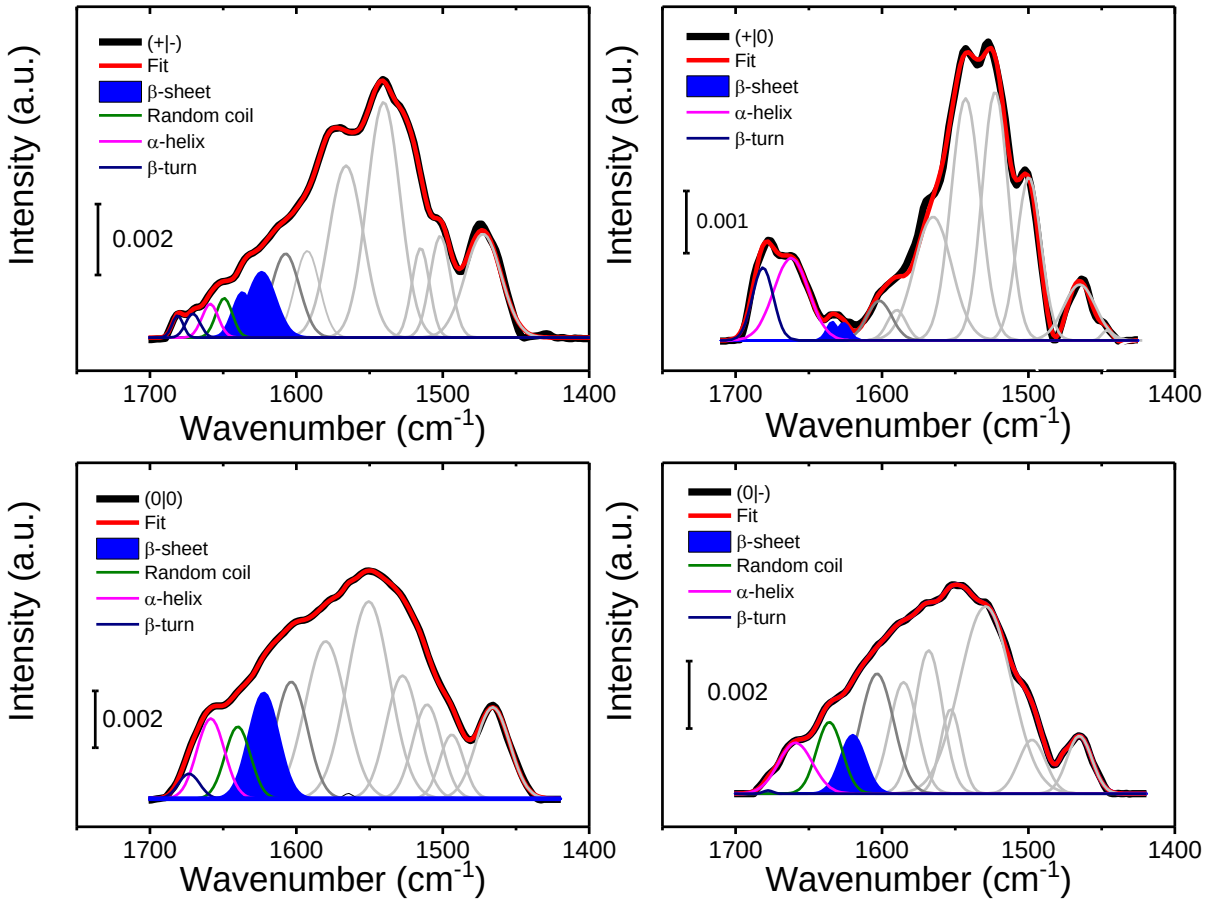

Figure S13. *Deconvolution of the PM-IRRA spectra in the amide I region recorded for the different hIAPP(20-29) fragments assembled at the OH-terminated SAM: native (upper left panel), amidated (upper right panel), acetylated and amidated (lower left panel) and acetylated (lower right panel), respectively. Black lines correspond to the experimental data while red lines represent the sums of the fitted components.*

Table S4. *Secondary structure contents obtained for the deconvolution of the PM-IRRA spectra registered for the different hIAPP(20-29) fragments assembled at the OH-terminated SAM.*

	Native (+|-)			
Component	**Position (cm^{-1})**	**Percentage (%)**	**total (%)**	**Amide I area**
β-sheet	1624	28.47	48.10	0.00694
β-sheet	1636	19.63		
Random coil	1650	17.15	20.97	
α-helix	1660	14.65	19.65	
β-turn	1670	10.43	20.04	
β-turn	1681	9.61		
	Amidated (+|0)			
Component	**Position (cm^{-1})**	**Percentage (%)**	**total (%)**	**Amide I area**
β-sheet	1625	4.43	8.65	0.08147
β-sheet	1635	4.22		
α-helix	1662	59.77	59.77	
β-turn	1681	31.57	31.57	
	Acetylated and amidated (0|0)			
Component	**Position (cm^{-1})**	**Percentage (%)**	**total (%)**	**Amide I area**
β-sheet	1622	40.77	40.77	0.23606
Random coil	1640	23.80	23.80	
α-helix	1657	28.57	28.57	
β-turn	1675	6.86	6.86	
	Acetylated (0|-)			
Component	**Position (cm^{-1})**	**Percentage (%)**	**total (%)**	**Amide I area**
β-sheet	1620	28.74	65.09	0.13093
β-sheet	1635	36.35		
α-helix/ R.coil	1658	34.31	34.31	
β-turn	1678	0.59	0.59	

Hydrophobic CH_3-terminated SAM

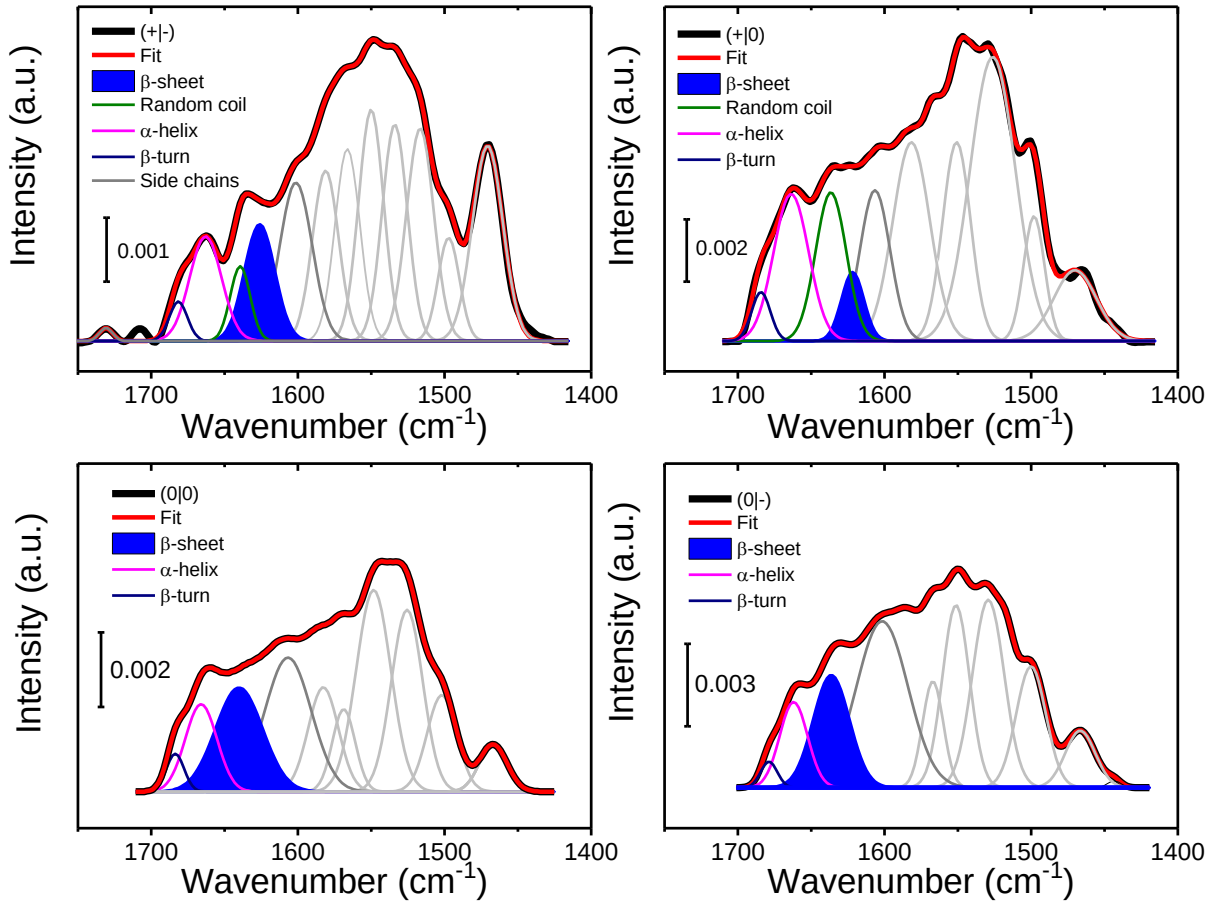

Figure S14. *Deconvolution of the PM-IRRA spectra in the amide I region recorded for the different hIAPP(20-29) fragments assembled at the CH_3-terminated SAM: native (upper left panel), amidated (upper right panel), acetylated and amidated (lower left panel) and acetylated (lower right panel), respectively. Black lines correspond to the experimental data while red lines represent the sums of the fitted components.*

Table S5. *Secondary structure contents obtained for the deconvolution of the PM-IRRA spectra registered for the different hIAPP(20-29) fragments assembled at the CH_3-terminated SAM.*

	Native (+|-)			
Component	**Position (cm^{-1})**	**Percentage (%)**	**total (%)**	**Amide I area**
β-sheet	1626	39.14	39.14	0.12799
Random coil	1640	16.29	16.29	
α-helix	1662	36.70	36.70	
β-turn	1681	7.87	7.87	
	Amidated (+|0)			
Component	**Position (cm^{-1})**	**Percentage (%)**	**total (%)**	**Amide I area**
β-sheet	1622	12.84	50.15	0.34197
β-sheet	1635	37.31		
α-helix	1663	42.30	42.30	
β-turn	1684	7.55	7.55	
β-sheet	-	0	0	
	Acetylated and amidated (0|0)			
Component	**Position (cm^{-1})**	**Percentage (%)**	**total (%)**	**Amide I area**
β-sheet	1636	58.89	58.89	0.19632
α-helix	1662	33.06	33.06	
β-turn	1681	8.05	8.05	
β-sheet	1695	0.05	0.05	
	Acetylated (0|-)			
Component	**Position (cm^{-1})**	**Percentage (%)**	**total (%)**	**Amide I area**
β-sheet	1634	59.30	59.30	0.21897
α-helix	1662	34.47	34.47	
β-turn	1680	6.23	6.23	
β-sheet	1690	0.1	0.1	

References

(1) Triulzi, R. C.; Li, C.; Naistat, D.; Orbulescu, J.; Leblanc, R. M. A Two-Dimensional Approach to Study Amyloid β-Peptide Fragment (25−35). *J. Phys. Chem. C* **2007**, *111*, 4661–4666, DOI: 10.1021/jp0669005.

(2) Desroches, M. J.; Chaudhary, N.; Omanovic, S. PM-IRRAS investigation of the interaction of serum albumin and fibrinogen with a biomedical-grade stainless steel 316LVM surface. *Biomacromolecules* **2007**, *8*, 2836–2844, DOI: 10.1021/bm070289d.

(3) Sarroukh, R.; Goormaghtigh, E.; Ruysschaert, J.-M.; Raussens, V. ATR-FTIR: a "rejuvenated" tool to investigate amyloid proteins. *Biochim. Biophys. Acta* **2013**, *1828*, 2328–2338, DOI: 10.1016/j.bbamem.2013.04.012.

(4) Yang, H.; Yang, S.; Kong, J.; Dong, A.; Yu, S. Obtaining information about protein secondary structures in aqueous solution using Fourier transform IR spectroscopy. *Nat. Protoc.* **2015**, *10*, 382–396, DOI: 10.1038/nprot.2015.024.

(5) Ruggeri, F. S.; Longo, G.; Faggiano, S.; Lipiec, E.; Pastore, A.; Dietler, G. Infrared nanospectroscopy characterization of oligomeric and fibrillar aggregates during amyloid formation. *Nat. Commun.* **2015**, *6*, 7831, DOI: 10.1038/ncomms8831.

(6) Cerf, E.; Sarroukh, R.; Tamamizu-Kato, S.; Breydo, L.; Derclaye, S.; Dufrêne, Y. F.; Narayanaswami, V.; Goormaghtigh, E.; Ruysschaert, J.-M.; Raussens, V. Antiparallel beta-sheet: a signature structure of the oligomeric amyloid beta-peptide. *Biochem. J.* **2009**, *421*, 415–423, DOI: 10.1042/BJ20090379.

(7) Sarroukh, R.; Cerf, E.; Derclaye, S.; Dufrêne, Y. F.; Goormaghtigh, E.; Ruysschaert, J.-M.; Raussens, V. Transformation of amyloid β(1-40) oligomers into fibrils is characterized by a major change in secondary structure. *Cell. Mol. Life Sci.* **2011**, *68*, 1429–1438, DOI: 10.1007/s00018-010-0529-x.

(8) Fortas, E.; Piccirilli, F.; Malabirade, A.; Militello, V.; Trépout, S.; Marco, S.; Taghbalout, A.; Arluison, V. New insight into the structure and function of Hfq C-terminus. *Biosci. Rep.* **2015**, *35,* DOI: 10.1042/BSR20140128.

(9) Moran, S. D.; Zanni, M. T. How to Get Insight into Amyloid Structure and Formation from Infrared Spectroscopy. *J. Phys. Chem. Lett.* **2014**, *5*, 1984–1993, DOI: 10.1021/jz500794d.

(10) Lomont, J. P.; Rich, K. L.; Maj, M.; Ho, J.-J.; Ostrander, J. S.; Zanni, M. T. Spectroscopic Signature for Stable β-Amyloid Fibrils versus β-Sheet-Rich Oligomers. *J. Phys. Chem. B* **2018**, *122*, 144–153, DOI: 10.1021/acs.jpcb.7b10765.